

# Deep DeePC: Data-enabled predictive control with low or no online optimization using deep learning

Xuwen Zhang<sup>a</sup>, Kaixiang Zhang<sup>b</sup>, Zhaojian Li<sup>b</sup>, Xunyuan Yin<sup>a,c,\*</sup>

<sup>a</sup>School of Chemistry, Chemical Engineering and Biotechnology, Nanyang Technological University, 62 Nanyang Drive, 637459, Singapore

<sup>b</sup>Department of Mechanical Engineering, Michigan State University, East Lansing, MI 48824, USA

<sup>c</sup> Environmental Process Modelling Centre, Nanyang Environment and Water Research Institute (NEWRI), Nanyang Technological University, 1 CleanTech Loop, 637141, Singapore

## Abstract

Data-enabled predictive control (DeePC) is a data-driven control algorithm that utilizes data matrices to form a non-parametric representation of the underlying system, predicting future behaviors and generating optimal control actions. DeePC typically requires solving an online optimization problem, the complexity of which is heavily influenced by the amount of data used, potentially leading to expensive online computation. In this paper, we leverage deep learning to propose a highly computationally efficient DeePC approach for general nonlinear processes, referred to as Deep DeePC. Specifically, a deep neural network is employed to learn the DeePC vector operator, which is an essential component of the non-parametric representation of DeePC. This neural network is trained offline using historical open-loop input and output data of the nonlinear process. With the trained neural network, the Deep DeePC framework is formed for online control implementation. At each sampling instant, this neural network directly outputs the DeePC operator, eliminating the need for online optimization as conventional DeePC. The optimal control action is obtained based on the DeePC operator updated by the trained neural network. To address constrained scenarios, a constraint handling scheme is further proposed and integrated with the Deep DeePC to handle hard constraints during online implementation. The efficacy and superiority of the proposed Deep DeePC approach are demonstrated using two benchmark process examples.

**Keywords:** Data-driven control, data-enabled predictive control, nonlinear process, computationally efficient controller.

---

\*Corresponding author: X. Yin. Tel: (+65) 6316 8746. Email: xunyuan.yin@ntu.edu.sg.

# 1 Introduction

Model predictive control (MPC) has been widely used for advanced process control of nonlinear industrial processes [1, 2]. Developing a nonlinear MPC typically requires a high-fidelity first-principles model that accurately describes the dynamic behavior of the underlying process [3–5]. Complex industrial processes are increasingly utilized across various fields to enhance operational efficiency, production consistency, and product quality [6–8]. The growing scale and structural complexity of these processes present significant challenges in developing nonlinear first-principles dynamic process models. Data-based optimal control offers a promising alternative for developing advanced control approaches for nonlinear processes without the need for an accurate first-principles model [9–15].

The Koopman theory-based framework [16] holds great promise for data-driven modeling and control of nonlinear systems. By constructing a linear model within a lifted state-space for a general nonlinear system from offline data, Koopman modeling facilitates the application of linear control theory to nonlinear systems and processes. Notable advancements include Koopman-based model predictive control (MPC) approaches [17–21], which develop linear MPC schemes for nonlinear systems, thereby maintaining convex online optimization despite the inherent nonlinearity of the underlying systems and processes. Koopman-based modeling and control have been widely applied across various fields, including industrial processes [22–25], vehicles and robotics [26–28], and power systems [29–31]. The development of Koopman MPC typically requires full-state feedback from the systems, with exceptions in [32, 33]. In [32], an input-output Koopman control method was proposed, where the Koopman-based controller only requires measurements of partial state variables directly used for calculating operational costs. In [33], a non-exact Koopman multi-step Koopman predictor was identified using only input and output data for the predictive control of nonlinear systems. We note that, in practical applications, measuring certain state variables can be challenging or costly. The need for full-state measurements poses significant challenges to the broader application of Koopman-based control methods in complex industrial systems.

In recent years, data-enabled predictive control (DeePC) has received increasing attention for its ability to address constrained optimal control using only input and output data [34–36]. DeePC leverages Willems’ fundamental lemma [37] to form a non-parametric representation of the system using a Hankel matrix established based on pre-collected input/output trajectories. Willems’ fundamental lemma indicates that any input/output trajectories of a linear system are spanned by the

Hankel matrix when the pre-collected input trajectory is persistently exciting [37]. DeePC produces the optimal control action by solving an optimization problem in a receding-horizon manner, which is similar to MPC [38].

DeePC utilizes gathered data to construct the Hankel matrix, with the dimension of the decision variable in the DeePC optimization problem being related to the dimension of this matrix. To satisfy the persistently exciting condition, a large amount of data is typically required to establish an accurate non-parametric representation of the system. Consequently, as the amount of used data increases, the computational complexity of the DeePC problem also increases, posing challenges for real-time application.

In the existing literature, efforts have been focused on addressing the computational challenges of DeePC by reducing the size or complexity of the Hankel matrix and optimization problems. In [39], singular value decomposition was leveraged on collected data to reduce the dimensionality of the DeePC problem, thus decreasing computational complexity. In [40], proper orthogonal decomposition was implemented to formulate a reduced order control problem, which was subsequently solved using a customized MPC solver. In [41, 42], LQ factorization was employed to redefine the decision variable, replacing the Hankel matrix with a lower triangular matrix. In [43], neighboring extremal was utilized to approximate the DeePC policy and reduce the computational cost for the constrained nonlinear systems. In [44], an online DeePC method was introduced using the primal-dual algorithm to solve the control problem recursively, coupled with the fast Fourier transform to expedite the computation of Hankel matrix-vector products. In [45], an alternative approach was proposed where DeePC is approximated by decomposing the original problem into two parts: a control objective and a scoring function. The scoring function is learned recursively from a size-invariant differentiable convex problem. While these existing methods improve the computational feasibility of DeePC, they still involve solving optimization problems or iterating algorithms during real-time applications, highlighting ongoing challenges in achieving real-time efficiency.

Motivated by these observations, this study aims to integrate deep learning methods with DeePC to eliminate the need to solve the online optimization problem at every sampling instant during the online implementation of a DeePC-based predictive controller. By leveraging a deep neural network, we learn the vector operator of DeePC from historical data collected from open-loop operations. The trained neural network outputs the vector operator without solving an optimization at each sampling instant during online implementation. Additionally, we develop a constraint handling scheme and integrate this scheme with the proposed optimization-free DeePC to address constrained

case scenarios. The proposed method is further slightly extended to address cases where reference inputs are unavailable. The proposed method is evaluated through two case studies on a gene regulatory network and a chemical process.

The contributions of this work and the main highlights of the proposed approach are summarized as follows:

- (a) We propose a deep learning-enabled DeePC method, referred to as Deep DeePC; this method does not need to solve any online optimization when constraints are either absent or not violated.
- (b) A constraint handling scheme is developed and integrated with Deep DeePC to realize constrained optimal control while maintaining a low optimization load.
- (c) The Deep DeePC control scheme can be trained using historical input and output data collected from open-loop process operations.
- (d) The proposed approach can be implemented even when reference inputs corresponding to the desired reference outputs are not given.
- (e) We use two benchmark nonlinear process examples to evaluate the performance of the proposed approach. Good control performance is achieved, and the computation time is significantly reduced as compared to conventional DeePC.

## 2 Preliminaries and problem formulation

### 2.1 Notation

$\mathbb{R}$  denotes the set of real numbers.  $\mathbb{Z}_{>0}$  and  $\mathbb{Z}_{\geq 0}$  denote the set of positive integers and the set of non-negative integers, respectively.  $\mathbb{E}$  denotes the expectation.  $\|x\|_Q^2$  is the square of the weighted Euclidean norm of vector  $x$  with positive-definite weighting matrix  $Q$ , computed as  $\|x\|_Q^2 := x^\top Q x$ .  $\text{diag}(\cdot)$  denotes a diagonal matrix.  $I_n$  is an identity matrix of dimension  $n$ .  $\odot$  denotes the Hadamard product.  $\mathbf{1}_{a < b}$  denotes an indicator function; it equals 1 if  $a < b$ , and equals 0 otherwise.  $\mathcal{U}(a, b)$  denotes a uniform distribution with lower and upper bounds  $a$  and  $b$ , respectively.  $x(i)$  denotes the  $i$ th variable of state vector  $x$ .  $x_k \in \mathbb{R}^{n_x}$  is the state vector at time instant  $k$ , and  $\{x\}_j^l := [x_j^\top, \dots, x_l^\top]^\top$  contains the state sequence from time instant  $j$  to  $l$ .

## 2.2 Non-parametric representation of linear systems

Consider a discrete linear time-invariant (LTI) system in which the dynamic behaviors are described by the following state-space form:

$$\begin{aligned} x_{k+1} &= Ax_k + Bu_k \\ y_k &= Cx_k + Du_k \end{aligned} \tag{1}$$

where  $x_k \in \mathbb{X} \subset \mathbb{R}^{n_x}$  is the system state vector;  $u_k \in \mathbb{U} \subset \mathbb{R}^{n_u}$  is the control input vector;  $y_k \in \mathbb{Y} \subset \mathbb{R}^{n_y}$  is the system output vector;  $A \in \mathbb{R}^{n_x \times n_x}$ ,  $B \in \mathbb{R}^{n_x \times n_u}$ ,  $C \in \mathbb{R}^{n_y \times n_x}$ , and  $D \in \mathbb{R}^{n_y \times n_u}$  are system matrices;  $\mathbb{X}$ ,  $\mathbb{U}$ , and  $\mathbb{Y}$  are compact sets.

Let  $L, T \in \mathbb{Z}_{>0}$  and  $T \geq L$ . Let  $\mathbf{u}_T^d := \{u^d\}_1^T \in \mathbb{R}^{n_u T}$  and  $\mathbf{y}_T^d := \{y^d\}_1^T \in \mathbb{R}^{n_y T}$  denote the input and output sequences for  $T$  time instants, respectively, with the superscript  $d$  indicating that the sequences are collected offline. For the input sequence  $\mathbf{u}_T^d$ , the Hankel matrix of depth  $L$  is defined as follows:

$$\mathcal{H}_L(\mathbf{u}_T^d) := \begin{bmatrix} u_1^d & u_2^d & \cdots & u_{T-L+1}^d \\ u_2^d & u_3^d & \cdots & u_{T-L+2}^d \\ \vdots & \vdots & \ddots & \vdots \\ u_L^d & u_{L+1}^d & \cdots & u_T^d \end{bmatrix} \tag{2}$$

where  $\mathcal{H}_L(\mathbf{u}_T^d) \in \mathbb{R}^{n_u L \times (T-L+1)}$ . Accordingly, for the controlled output sequence  $\mathbf{y}_T^d$ , define the Hankel matrix  $\mathcal{H}_L(\mathbf{y}_T^d) \in \mathbb{R}^{n_y L \times (T-L+1)}$ . Next, we introduce the concept of persistent excitation and Willems' fundamental lemma [37].

**Definition 1** *Let  $T, L \in \mathbb{Z}_{>0}$  and  $T \geq L$ . The input sequence  $\mathbf{u}_T := \{u\}_1^T$  is persistently exciting of order  $L$ , if  $\mathcal{H}_L(\mathbf{u}_T)$  is of full row rank.*

**Lemma 1** *(Willems' fundamental lemma [37]) Consider an LTI system (1) and assume this system is controllable. Consider that  $\mathbf{u}_T^d := \{u^d\}_1^T \in \mathbb{R}^{n_u T}$  and  $\mathbf{y}_T^d := \{y^d\}_1^T \in \mathbb{R}^{n_y T}$  are the  $T$ -step input and output sequences for system (1), respectively, and the input sequence  $\mathbf{u}_T^d$  is persistently exciting of order  $L + n_x$ . Any  $L$ -step sequences  $\mathbf{u}_L := \{u\}_1^L \in \mathbb{R}^{n_u L}$  and  $\mathbf{y}_L := \{y\}_1^L \in \mathbb{R}^{n_y L}$  are the input and output trajectories of system (1), if and only if*

$$\begin{bmatrix} \mathcal{H}_L(\mathbf{u}_T^d) \\ \mathcal{H}_L(\mathbf{y}_T^d) \end{bmatrix} g = \begin{bmatrix} \mathbf{u}_L \\ \mathbf{y}_L \end{bmatrix} \tag{3}$$

for vector  $g \in \mathbb{R}^{T-L+1}$ .

A persistently exciting input sequence should be sufficiently rich and of sufficient length to excite the system. This produces an output sequence that is sufficient to represent the behavior of the underlying system. Based on Lemma 1, a non-parametric representation of the system (1) can be formulated using finite input and output sequences when the input sequence is persistently exciting.

### 2.3 Data-enabled predictive control (DeePC)

Data-enabled predictive control (DeePC) [34] is a data-based control approach that creates a non-parametric representation of the underlying system using pre-collected input and output data. This way, system identification/modeling can be bypassed.

Lemma 1 allows for the description of the dynamic behaviors of the system using data collected offline. Let  $T_{ini}, N_p \in \mathbb{Z}_{>0}$  and  $L = T_{ini} + N_p$ . Any  $L$ -step input and output sequence of the system (1) can be expressed using pre-collected data. To conduct an  $N_p$ -step prediction, the Hankel matrices  $\mathcal{H}_L(\mathbf{u}_T^d)$  and  $\mathcal{H}_L(\mathbf{y}_T^d)$  are partitioned into two parts, that is, the past data of length  $T_{ini}$  and the future data of length  $N_p$ , described as follows:

$$\begin{bmatrix} U_p \\ U_f \end{bmatrix} := \mathcal{H}_L(\mathbf{u}_T^d), \quad \begin{bmatrix} Y_p \\ Y_f \end{bmatrix} := \mathcal{H}_L(\mathbf{y}_T^d) \quad (4)$$

where  $U_p \in \mathbb{R}^{n_u T_{ini} \times (T-L+1)}$  denotes the past data which consist of the first  $n_u T_{ini}$  block rows of  $\mathcal{H}_L(\mathbf{u}_T^d)$ ;  $U_f \in \mathbb{R}^{n_u N_p \times (T-L+1)}$  denotes the future data which consist of the last  $n_u N_p$  block rows of  $\mathcal{H}_L(\mathbf{u}_T^d)$  (similarly for  $Y_p$  and  $Y_f$ ).

In online implementation, at time instant  $k$ , let  $\mathbf{u}_{ini,k} := \{u\}_{k-T_{ini}}^{k-1}$  and  $\mathbf{y}_{ini,k} := \{y\}_{k-T_{ini}}^{k-1}$  be the  $T_{ini}$ -step input and output sequences before the current time instant  $k$ , respectively. Let  $\hat{\mathbf{u}}_k := \{\hat{u}\}_{k|k}^{k+N_p-1|k}$  and  $\hat{\mathbf{y}}_k := \{\hat{y}\}_{k|k}^{k+N_p-1|k}$  be the future  $N_p$ -step input and output prediction, where  $\hat{u}_{j|k}$  and  $\hat{y}_{j|k}$  represent the predicted input and output for time instant  $j$  obtained at time instant  $k$ , respectively. Based on Willems' fundamental lemma,  $\mathbf{u}_{ini,k}$ ,  $\mathbf{y}_{ini,k}$ ,  $\hat{\mathbf{u}}_k$ , and  $\hat{\mathbf{y}}_k$  sequences belong to the system (1), if and only if there exists a vector  $g_k$  at time instant  $k$  such that:

$$\begin{bmatrix} U_p \\ Y_p \\ U_f \\ Y_f \end{bmatrix} g_k = \begin{bmatrix} \mathbf{u}_{ini,k} \\ \mathbf{y}_{ini,k} \\ \hat{\mathbf{u}}_k \\ \hat{\mathbf{y}}_k \end{bmatrix} \quad (5)$$

The vector  $g_k$  in (5) is referred to as ‘‘DeePC operator’’ in the remainder of this paper. The initial input and output trajectories,  $\mathbf{u}_{ini,k}$  and  $\mathbf{y}_{ini,k}$ , determine the initial state  $x_k$  of the underlying system, which is the starting point for the future trajectories [34, 46].

Based on (5), the optimization problem associated with DeePC at time instant  $k$  can be formulated as follows:

$$\min_{g_k, \hat{\mathbf{u}}_k, \hat{\mathbf{y}}_k} \|\hat{\mathbf{y}}_k - \mathbf{y}_k^r\|_Q^2 + \|\hat{\mathbf{u}}_k - \mathbf{u}_k^r\|_R^2 \quad (6a)$$

$$\text{s.t.} \quad \begin{bmatrix} U_p \\ Y_p \\ U_f \\ Y_f \end{bmatrix} g_k = \begin{bmatrix} \mathbf{u}_{ini,k} \\ \mathbf{y}_{ini,k} \\ \hat{\mathbf{u}}_k \\ \hat{\mathbf{y}}_k \end{bmatrix} \quad (6b)$$

$$\hat{u}_{j|k} \in \mathbb{U}, \quad j = k, \dots, k + N_p - 1 \quad (6c)$$

$$\hat{y}_{j|k} \in \mathbb{Y}, \quad j = k, \dots, k + N_p - 1 \quad (6d)$$

where  $\mathbf{y}_k^r := \{y^r\}_k^{k+N_p-1} \in \mathbb{R}^{n_y N_p}$  and  $\mathbf{u}_k^r := \{u^r\}_k^{k+N_p-1} \in \mathbb{R}^{n_u N_p}$  are the reference trajectories of controlled output and control input, respectively;  $Q \in \mathbb{R}^{n_y N_p \times n_y N_p}$  and  $R \in \mathbb{R}^{n_u N_p \times n_u N_p}$  are tunable weighting matrices.

In the online implementation, DeePC solves (6) in a receding horizon manner [34, 39]. Specifically, at sampling instant  $k$ ,  $k \in \mathbb{Z}_{\geq 0}$ , the optimal DeePC operator  $g_k^*$ , optimal control input sequence  $\hat{\mathbf{u}}_k^*$ , and optimal predicted output trajectory  $\hat{\mathbf{y}}_k^*$  are obtained by solving (6), and the first control action  $\hat{u}_{k|k}^*$  in the optimal control sequence  $\hat{\mathbf{u}}_k^* = [\hat{u}_{k|k}^{*\top}, \dots, \hat{u}_{k+N_p-1|k}^{*\top}]^\top$  will be applied to the system to achieve desired control performance. At the next sampling instant  $k + 1$ ,  $\mathbf{u}_{ini,k+1}$  and  $\mathbf{y}_{ini,k+1}$  are updated with the applied input and measured output data,  $u_k$  and  $y_k$ , from the previous time instant  $k$ , respectively.

## 2.4 Problem formulation

In this work, we consider discrete-time nonlinear systems of which the dynamics can be described by the following state-space form:

$$x_{k+1} = f(x_k, u_k) \quad (7a)$$

$$y_k = Cx_k \quad (7b)$$

where  $x_k \in \mathbb{X} \subset \mathbb{R}^{n_x}$  is the system state vector;  $u_k \in \mathbb{U} \subset \mathbb{R}^{n_u}$  is the control input vector;  $y_k \in \mathbb{Y} \subset \mathbb{R}^{n_y}$  is the output measurement vector;  $f : \mathbb{X} \times \mathbb{U} \rightarrow \mathbb{X}$  is a nonlinear function that characterizes the state dynamics of the process;  $C \in \mathbb{R}^{n_y \times n_x}$  is the system matrix; and  $\mathbb{X}$ ,  $\mathbb{U}$ , and  $\mathbb{Y}$  are compact sets. We consider nonlinear systems in which the output measurements linearly depend on the state vectors. Our objective is to address the control for the nonlinear processes using only input and output data in an efficient manner within the DeePC framework.

Similar to model predictive control, a conventional DeePC-based controller needs to solve online optimization in a receding horizon manner at every new sampling instant [34, 39]. The optimization problem associated with DeePC can be computationally complex, although DeePC typically formulates convex optimization [39, 40, 45]. Based on this consideration, in this work, we aim to propose an efficient DeePC method that requires low optimization/no optimization during online implementation.

To achieve this objective, we propose to use a deep neural network to approximate the DeePC operator  $g$  of the non-parametric formulation in (5). Historical open-loop data are used for the training of the deep neural network, and are formulated into initial and reference trajectories following the DeePC framework. Once the training is completed, the neural network will output the values of the DeePC operator  $g$  at each sampling instant without solving the optimization in the form of (6).

Additionally, to handle the cases when the control action generated by the deep neural network leads to constraint violations, we propose a constraint handling scheme to ensure that the input and output constraints of the system are maintained during online implementation.

### 3 Applicability of DeePC for nonlinear systems

We will use the conventional DeePC described in (6) as the foundation of developing our deep learning-enabled DeePC method. Given that (6) was originally developed for LTI systems based on Lemma 1, in this section, we leverage the concept of Koopman modeling for control to justify the appropriateness of using conventional DeePC in (6) as the basis for developing DeePC-based controllers for nonlinear systems in (7).

Consider a discrete-time nonlinear control system described in (7). Based on the Koopman theory for controlled systems, the state vector can be extended to include control inputs, that is,  $\chi_k = [x_k^\top, u_k^\top]^\top$  [17]. Accordingly, there exists an infinite-dimensional nonlinear lifting mapping

$\Psi_\chi$  that allows the dynamics of the lifted state to be governed by a Koopman operator  $\mathcal{K}$  as follows [17, 21, 47]:

$$\Psi_\chi(\chi_{k+1}) = \mathcal{K}\Psi_\chi(\chi_k) \quad (8)$$

where  $\Psi_\chi(\chi_k) := [\Psi(x_k)^\top, u_k^\top]^\top$  with  $\Psi$  being a nonlinear mapping for the system state  $x$ . The corresponding Koopman operator  $\mathcal{K}$  can then be identified and represented as a block matrix as follows:

$$\mathcal{K} = \begin{bmatrix} A_{\mathcal{K}} & B_{\mathcal{K}} \\ \text{---} & \text{---} \\ * & * \end{bmatrix}. \quad (9)$$

Since the primary focus is on the future behaviors of the lifted state  $\Psi$  (which are directly related to the original system states  $x$ ) instead of all the elements of  $\Psi_\chi$ , it is sufficient only to identify matrices  $A_{\mathcal{K}}$  and  $B_{\mathcal{K}}$ . In addition, a projection matrix  $D_{\mathcal{K}}$  is used to map the lifted state  $\Psi$  back to the original state space. The Koopman-based linear model for nonlinear control system (7) can be described as follows [17, 21–23]:

$$\Psi(x_{k+1}) = A_{\mathcal{K}}\Psi(x_k) + B_{\mathcal{K}}u_k \quad (10a)$$

$$\hat{x}_k = D_{\mathcal{K}}\Psi(x_k) \quad (10b)$$

Let  $z = \Psi(x) \in \mathbb{R}^{n_z}$  represent the lifted state vector. A Koopman-based LTI model can be constructed in the following form [48]:

$$z_{k+1} = A_{\mathcal{K}}z_k + B_{\mathcal{K}}u_k \quad (11a)$$

$$\hat{x}_k = D_{\mathcal{K}}z_k \quad (11b)$$

$$y_k = C_z z_k \quad (11c)$$

where  $C_z = CD_{\mathcal{K}}$  is the output measurement matrix. (11) characterizes (or more precisely, approximates) the dynamic behaviors of the original nonlinear system in (7) in a higher-dimensional space. It is worth noting that the established Koopman-based LTI model in (11) has the same control input  $u$  and output measurements  $y$  as the underlying nonlinear system in (7). This implies that for the nonlinear process (7), there exists a higher-dimensional LTI model that can represent or approximate the nonlinear dynamics of the underlying system, with control inputs and measured outputs remaining unaffected by coordinate changes, thereby retaining their original physical

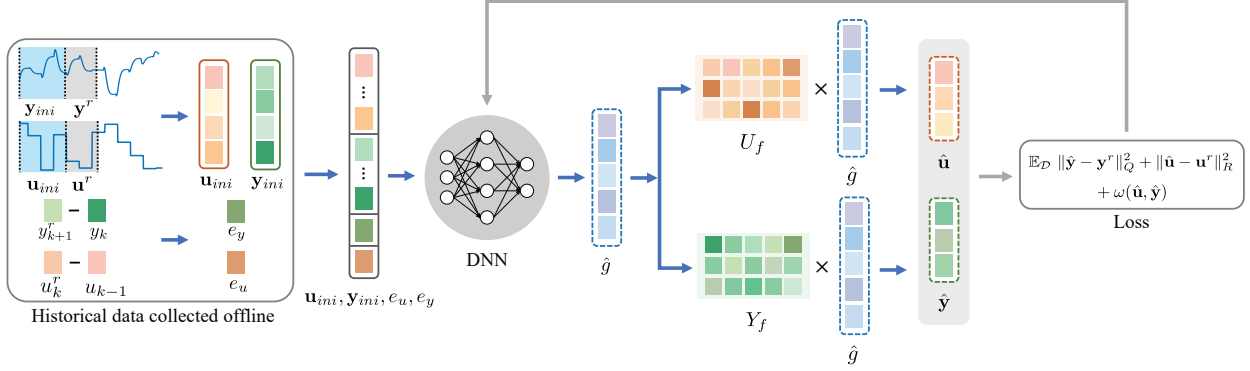


Figure 1: A graphical illustration of the proposed deep learning-enabled DeePC pipeline.

meaning.

For any DeePC method that can be applied to the LTI model in (11), it is almost equivalent to apply the same DeePC method to the underlying nonlinear system in (7). On the other hand, based on Willems' fundamental lemma, if the established Koopman-based LTI model in its lifted space is controllable, a DeePC controller can be formulated following (6). This supports the appropriateness of applying DeePC-based methods that were originally developed for LTI systems, including the conventional DeePC in (6), to the nonlinear system in (7), particularly from a Koopman-based modeling and control perspective.

## 4 Deep learning-based DeePC control approach

In this section, we propose the deep learning-based DeePC method – Deep DeePC, which leverages deep learning to generate optimal control actions without the need to solve the optimization problem (6) at each sampling instant during online implementation. In addition, the process of constructing a training data set for Deep DeePC using historical offline data is explained.

### 4.1 Structure of the proposed method

A graphical illustration of the proposed Deep DeePC pipeline is presented in Figure 1. Historical open-loop data are utilized to construct a dataset, which is used to train a dense neural network (DNN). This DNN is leveraged to output an approximation of the DeePC operator  $g$  in the non-parametric model in (5), based on the constructed training data from the open-loop data. The trajectories of future inputs and system outputs, denoted by  $\hat{\mathbf{u}}$  and  $\hat{\mathbf{y}}$ , will be predicted based on the output of the DNN and (5). The objective is to train the DNN such that future system outputs

are driven towards the reference trajectories.

## 4.2 Deep DeePC

By incorporating the equality constraints  $\hat{\mathbf{u}}_k = U_f g_k$  and  $\hat{\mathbf{y}}_k = Y_f g_k$  from (6b) into the objective function (6a), the online optimization problem for DeePC in (6) are re-formulated as follows [43]:

$$\min_{g_k} \|Y_f g_k - \mathbf{y}_k^r\|_Q^2 + \|U_f g_k - \mathbf{u}_k^r\|_R^2 \quad (12a)$$

$$\text{s.t.} \quad \begin{bmatrix} U_p \\ Y_p \end{bmatrix} g_k = \begin{bmatrix} \mathbf{u}_{ini,k} \\ \mathbf{y}_{ini,k} \end{bmatrix} \quad (12b)$$

$$\hat{\mathbf{u}}_{j|k} \in \mathbb{U}, \quad j = k, \dots, k + N_p - 1 \quad (12c)$$

$$\hat{\mathbf{y}}_{j|k} \in \mathbb{Y}, \quad j = k, \dots, k + N_p - 1 \quad (12d)$$

This way, the decision variable of the online optimization problem for DeePC has reduced from  $g_k$ ,  $\hat{\mathbf{u}}_k$ , and  $\hat{\mathbf{y}}_k$  to just the DeePC operator  $g_k$ .

In this work, we aim to realize online DeePC-based control of the nonlinear process in a manner that bypasses solving the online optimization in (12). In the optimization problem (12), the Hankel matrices  $U_p$  and  $Y_p$ , constructed from offline open-loop process operation data, remain unchanged during each time instant update. Therefore, the elements of DeePC operator  $g_k$ , which are the decision variables of the DeePC formulation in (12), are determined at each sampling instant  $k, k \in \mathbb{Z}_{\geq 0}$ , based on the initial trajectories of the inputs and the outputs, denoted by  $\mathbf{u}_{ini,k}$  and  $\mathbf{y}_{ini,k}$ .

As depicted in Figure 1, a neural network, denoted by  $F_\theta$ , is trained, and the trained neural network will update the DeePC operator  $g_k$  at each new sampling instant during online implementation. The structure of this neural network is designed as follows:

$$\hat{g}_k = F_\theta(\mathbf{u}_{ini,k}, \mathbf{y}_{ini,k}, e_{u,k}, e_{y,k} | \theta) \quad (13)$$

where  $\hat{g}_k$  is the predicted DeePC operator and  $\theta$  includes the trainable parameters of neural network  $F_\theta$ . The inputs to  $F_\theta$  include the initial input and output trajectories, that is,  $\mathbf{u}_{ini,k}$  and  $\mathbf{y}_{ini,k}$ . Additionally, to enable set-point tracking capability of the proposed Deep DeePC method, the input and output tracking errors between the future and current time instant are also incorporated as inputs to this neural network. Specifically, the input error is the difference between the reference

input at current time instant  $k$  and the control input at previous time instant  $k - 1$ , i.e.,  $e_{u,k} = u_k^r - u_{k-1}$ , and the output error is the difference between the reference output at time instant  $k + 1$  and the latest measured output at time instant  $k$ , i.e.,  $e_{y,k} = y_{k+1}^r - y_k$ . The time instants for the input and output errors are different because the system output is one step ahead of the input. The dimension of the inputs to the neural network  $F_\theta$  is determined based on the selected parameters  $T_{ini}$  for DeePC design and the system parameters  $n_u$  and  $n_y$ , resulting in a dimension of  $(n_u + n_y) \times (T_{ini} + 1)$ . The dimension of the output of  $F_\theta$  is the same as the dimension of DeePC operator  $g_k$  in (12), which is  $T - T_{ini} - N_p + 1$ .

The objective of this neural network is to output DeePC operator  $\hat{g}_k$ , which can be further used to generate control actions that drive the system towards desired reference outputs – this control objective aligns with that of DeePC (12a). To address the input and output constraints, a soft constraint  $\omega(\hat{\mathbf{u}}, \hat{\mathbf{y}})$  is incorporated into the objective function. Given a dataset  $\mathcal{D}$  composed of multiple  $T_{ini}$ -step initial input and output trajectories,  $\mathbf{u}_{ini}$  and  $\mathbf{y}_{ini}$ , and their corresponding  $N_p$ -step input and reference outputs,  $\mathbf{u}^r$  and  $\mathbf{y}^r$ , the objective function used to train the parameters in  $\theta$  is as follows:

$$\mathcal{L} = \mathbb{E}_{\mathcal{D}} \|\hat{\mathbf{y}} - \mathbf{y}^r\|_Q^2 + \|\hat{\mathbf{u}} - \mathbf{u}^r\|_R^2 + \omega(\hat{\mathbf{u}}, \hat{\mathbf{y}}) \quad (14a)$$

$$= \mathbb{E}_{\mathcal{D}} \|Y_f \hat{g} - \mathbf{y}^r\|_Q^2 + \|U_f \hat{g} - \mathbf{u}^r\|_R^2 + \omega(U_f \hat{g}, Y_f \hat{g}) \quad (14b)$$

where  $\hat{\mathbf{u}}$  and  $\hat{\mathbf{y}}$  are the predicted future input/output trajectories based on the DeePC operator  $\hat{g}$  generated by the neural network. The soft constraint  $\omega(\hat{\mathbf{u}}, \hat{\mathbf{y}})$  is described as follows:

$$\omega(\hat{\mathbf{u}}, \hat{\mathbf{y}}) = \|\hat{\mathbf{u}} - \mathbf{u}_{lb}\|_{P'_{u,lb}}^2 + \|\mathbf{u}_{ub} - \hat{\mathbf{u}}\|_{P'_{u,ub}}^2 + \|\hat{\mathbf{y}} - \mathbf{y}_{lb}\|_{P'_{y,lb}}^2 + \|\mathbf{y}_{ub} - \hat{\mathbf{y}}\|_{P'_{y,ub}}^2 \quad (15)$$

where  $\mathbf{u}_{lb} \in \mathbb{R}^{n_u N_p}$  and  $\mathbf{u}_{ub} \in \mathbb{R}^{n_u N_p}$  are the lower and upper bounds of the input variables for  $N_p$  steps, respectively (similarly for  $\mathbf{y}_{lb}$  and  $\mathbf{y}_{ub}$ ).  $P'_{u,lb} = P_u \odot M_{u,lb} \in \mathbb{R}^{n_u N_p \times n_u N_p}$  and  $P'_{u,ub} = P_u \odot M_{u,ub} \in \mathbb{R}^{n_u N_p \times n_u N_p}$  where  $P_u$  is the weighting matrix of the term that penalizes the violation of input constraint;  $M_{u,lb} = \text{diag}([\mathbf{1}_{\hat{\mathbf{u}}(1) < \mathbf{u}_{lb}(1)}, \dots, \mathbf{1}_{\hat{\mathbf{u}}(n_u N_p) < \mathbf{u}_{lb}(n_u N_p)}])$  and  $M_{u,ub} = \text{diag}([\mathbf{1}_{\mathbf{u}_{ub}(1) < \hat{\mathbf{u}}(1)}, \dots, \mathbf{1}_{\mathbf{u}_{ub}(n_u N_p) < \hat{\mathbf{u}}(n_u N_p)}])$  are the mask matrices used to penalize the violated terms (similarly for  $P'_{y,lb}$  and  $P'_{y,ub}$ ).

The optimization problem associated with the offline neural network training can be formulated

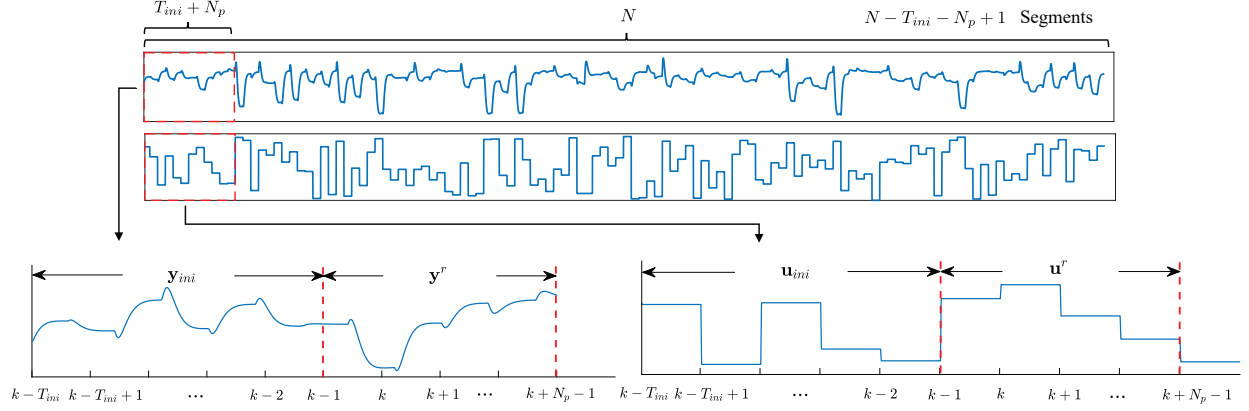


Figure 2: A graphical illustration of the construction of training data based on system historical data collected offline.

as follows:

$$\min_{\theta} \mathcal{L} = \min_{\theta} \mathbb{E}_{\mathcal{D}} \|Y_f \hat{g} - \mathbf{y}^r\|_Q^2 + \|U_f \hat{g} - \mathbf{u}^r\|_R^2 + \omega(U_f \hat{g}, Y_f \hat{g}) \quad (16)$$

where  $\hat{g} = F_{\theta}(\mathbf{u}_{ini}, \mathbf{y}_{ini}, e_u, e_y | \theta)$ .

Once the training is completed, the trained neural network  $F_{\theta}$  is used to output DeePC operator  $\hat{g}_k$  online following (13), at each sampling time instant  $k$ ,  $k \in \mathbb{Z}_{\geq 0}$ . The DeePC operator  $\hat{g}_k$  is then used to generate the optimal control sequence  $\hat{\mathbf{u}}_k^*$  following:

$$\hat{\mathbf{u}}_k^* = U_f \hat{g}_k = U_f F_{\theta}(\mathbf{u}_{ini,k}, \mathbf{y}_{ini,k}, e_{u,k}, e_{y,k} | \theta^*) \quad (17)$$

where  $\theta^*$  is the optimal neural network parameters after training. The first control action  $\hat{u}_{k|k}^*$  in  $\hat{\mathbf{u}}_k^*$  will be applied to the system to achieve desired control objectives. It is worth noting that the proposed Deep DeePC method is free of online optimization, once the neural network is fully trained offline.

### 4.3 Training data construction

Training the neural network in (13) based on the objective function in (14) requires a data set that comprises initial input and initial output trajectories (denoted by  $\mathbf{u}_{ini}$  and  $\mathbf{y}_{ini}$ , respectively), and their corresponding future input and reference outputs (denoted by  $\mathbf{u}^r$  and  $\mathbf{y}^r$ , respectively). The initial input and output trajectories are used as inputs to the neural network in (13), while the future references serve as the labels that are used to compute the values of the objective function, as needed for supervised learning-based training as described in (14). The combined initial trajectories

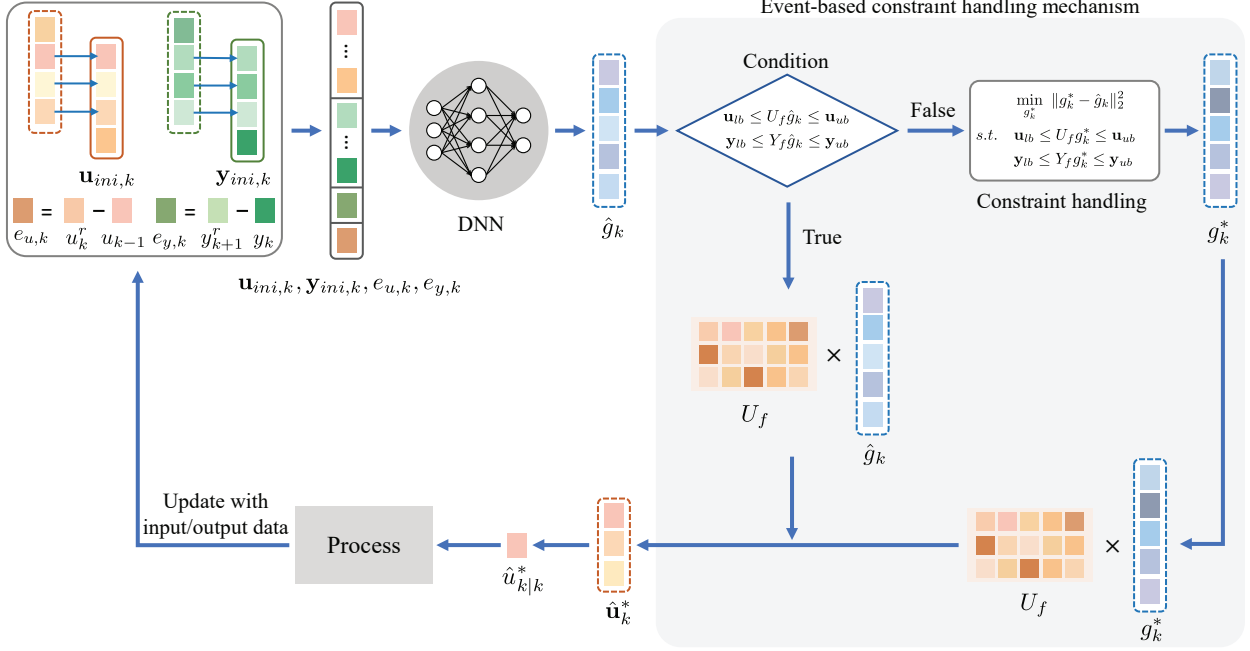


Figure 3: A block diagram of the online implementation of the proposed deep learning-enabled DeePC design with an event-based constraint handling scheme.

and future references should consist of samples collected at consecutive time instants that span a specific  $(T_{ini} + N_p)$ -step time window. In this work, we utilize historical data to construct the input and label data for training the neural network.

Figure 2 provides a graphical illustration of the construction of a training data set based on historical data of the system collected offline. The objective is to construct  $(T_{ini} + N_p)$ -step continuous sequences, which can then be divided into input and label data for neural network training. As shown in Figure 2,  $(N - T_{ini} - N_p + 1)$  segments of the  $(T_{ini} + N_p)$ -step sequences can be extracted from an  $N$ -step sequential system trajectory. Within each segment, the first  $T_{ini}$  steps of the segment are treated as the initial trajectories  $\mathbf{u}_{ini}$  and  $\mathbf{y}_{ini}$  which are the input of the neural network, and the remaining  $N_p$  steps of the segment are regarded as the future references  $\mathbf{u}^r$  and  $\mathbf{y}^r$  corresponding to the initial trajectories which are the labels of the supervised learning. In addition, the input and output errors,  $e_u$  and  $e_y$ , are computed by the constructed initial trajectories and future references of the selected segment based on (13).

## 5 Event-based constraint handling

The proposed Deep DeePC in Section 4.2 is highly computationally efficient since it does not require solving online optimization. Meanwhile, it is worth mentioning that the Deep DeePC controller in (17) is not capable of handling hard constraints on either the system inputs or the system outputs. To deal with cases when constraint satisfaction is critical, for example, when safety-related constraints need to be satisfied, we further propose an event-based constraint handling scheme. This scheme can be incorporated into the proposed online optimization-free Deep DeePC (17) to ensure the satisfaction of input and output constraints during online implementation, when it is necessary. An illustrative diagram of the Deep DeePC approach with the constraint handling scheme is presented in Figure 3.

The online implementation of Deep DeePC with the constraint handling scheme is described in Algorithm 1. At each sampling instant  $k$ ,  $k \in \mathbb{Z}_{\geq 0}$ , the trained DNN model generates the DeePC operator  $\hat{g}_k$  based on the  $\mathbf{u}_{ini,k}$ ,  $\mathbf{y}_{ini,k}$ ,  $e_{u,k}$ ,  $e_{y,k}$  collected during online operation:

$$\hat{g}_k = F_{\theta}(\mathbf{u}_{ini,k}, \mathbf{y}_{ini,k}, e_{u,k}, e_{y,k} | \theta^*) \quad (18)$$

Then future optimal control sequence  $\hat{\mathbf{u}}_k$  can be obtained based on (17), and the corresponding future output trajectories  $\hat{\mathbf{y}}_k$  can be computed following DeePC framework, i.e.,  $\hat{\mathbf{y}}_k = Y_f \hat{g}_k$ .

The predicted future input and output trajectories generated based on  $\hat{g}_k$  in (18) may not always satisfy the hard constraints. In such cases, if any of the predicted future states violate the constraints, a constraint handling scheme is proposed to adjust the DeePC operator  $\hat{g}_k$  to comply with the constraints. The objective of this design is to find an optimized DeePC operator  $g_k^*$  which is close to  $\hat{g}_k$  while ensuring that the future states meet the system constraints. The optimization problem is formulated as follows:

$$\min_{g_k^*} \|g_k^* - \hat{g}_k\|_2^2 \quad (19a)$$

$$\text{s.t. } \mathbf{u}_{lb} \leq U_f g_k^* \leq \mathbf{u}_{ub} \quad (19b)$$

$$\mathbf{y}_{lb} \leq Y_f g_k^* \leq \mathbf{y}_{ub} \quad (19c)$$

We note that if the predicted future  $N_p$ -step input and output trajectories do not violate the system constraints, then (19) does not need to be solved, and the optimal control sequence generated

---

**Algorithm 1:** Online implementation of Deep DeePC with constraint handling scheme
 

---

**Input:** Trained neural network  $F_\theta$  with optimized parameters  $\theta^*$ ; established Hankel matrices  $U_f$  and  $Y_f$  based on offline collected data  $\mathbf{u}_T^d$  and  $\mathbf{y}_T^d$ ; steady-state input and reference outputs  $\mathbf{u}^r$  and  $\mathbf{y}^r$ .

**Output:** Real-time input and output trajectories.

```

1 Initialize  $\mathbf{u}_{ini,T_{ini}}, \mathbf{y}_{ini,T_{ini}}, e_{u,T_{ini}},$  and  $e_{y,T_{ini}}$ .
2 while  $k > T_{ini}$  do
    2.1 Compute the DeePC operator following  $\hat{g}_k = F_\theta(\mathbf{u}_{ini,k}, \mathbf{y}_{ini,k}, e_{u,k}, e_{y,k} | \theta^*)$ .
    2.2 if  $\mathbf{u}_{lb} \leq U_f \hat{g}_k \leq \mathbf{u}_{ub}$  and  $\mathbf{y}_{lb} \leq Y_f \hat{g}_k \leq \mathbf{y}_{ub}$  then
        | Compute the optimal control sequence following  $\hat{\mathbf{u}}_k^* = U_f \hat{g}_k$ .
    else
        | Solve optimization problem (19) to update DeePC operator  $g_k^*$ .
        | Compute the optimal control sequence following  $\hat{\mathbf{u}}_k^* = U_f g_k^*$ .
    end
    2.3 Apply  $u_k$  where  $u_k = \hat{u}_{k|k}^*$  to the process in (7).
    2.4 Update  $\mathbf{u}_{ini,k+1} := \{u\}_{k-T_{ini}+1}^k, \mathbf{y}_{ini,k+1} := \{y\}_{k-T_{ini}+1}^k$ .
    2.5 Update  $e_{u,k+1} = u_{k+1}^r - u_k, e_{y,k+1} = y_{k+2}^r - y_{k+1}$ .
    2.6  $k \leftarrow k + 1$ .
end
  
```

---

based on (17) can be directly obtained based on  $\hat{g}_k$ . The optimal control sequence  $\hat{\mathbf{u}}_k^*$  for  $N_p$  steps can be obtained and described as follows:

$$\hat{\mathbf{u}}_k^* = \begin{cases} U_f \hat{g}_k, & \text{if } \mathbf{u}_{lb} \leq U_f \hat{g}_k \leq \mathbf{u}_{ub} \text{ and } \mathbf{y}_{lb} \leq Y_f \hat{g}_k \leq \mathbf{y}_{ub} \\ U_f g_k^*, & \text{otherwise} \end{cases} \quad (20)$$

The first control action  $\hat{u}_{k|k}^*$  in the optimal control sequence  $\hat{\mathbf{u}}_k^*$  is applied to the system to achieve the desired control performance.

## 6 Extension of the proposed method

In this section, we present an alternative method to extend our proposed Deep DeePC approach to handle situations where steady-state reference inputs are unavailable for the nonlinear process

under consideration.

The online implementation of the well-trained Deep DeePC model for control tasks requires information on the initial input and output trajectories,  $\mathbf{u}_{ini}$  and  $\mathbf{y}_{ini}$ , along with the input and output errors,  $e_u$  and  $e_y$ . However, in some cases where the steady-state reference inputs corresponding to the set-points are unknown, implementing the current approach becomes impractical. Therefore, an alternative design for Deep DeePC is proposed that does not require steady-state reference inputs.

The neural network is described as follows:

$$\hat{g}_k = \tilde{F}_{\tilde{\theta}}(\mathbf{u}_{ini,k}, \mathbf{y}_{ini,k}, e_{y,k} | \tilde{\theta}) \quad (21)$$

where  $\tilde{F}_{\tilde{\theta}}$  denotes the neural network without the input of steady-state reference input;  $\tilde{\theta}$  denotes the trainable parameters of neural network  $\tilde{F}_{\tilde{\theta}}$ . The input dimension of the neural network  $\tilde{F}_{\tilde{\theta}}$  is reduced to  $(n_u + n_y) \times T_{ini} + n_y$ . Given a data set  $\tilde{\mathcal{D}}$  that composed of multiple  $\mathbf{u}_{ini}$ ,  $\mathbf{y}_{ini}$ , and corresponding  $\mathbf{y}^r$ , the objective function used to train the neural network  $\tilde{F}_{\tilde{\theta}}$  is:

$$\tilde{\mathcal{L}} = \mathbb{E}_{\tilde{\mathcal{D}}} \|\hat{\mathbf{y}} - \mathbf{y}^r\|_Q^2 + \omega(\hat{\mathbf{u}}, \hat{\mathbf{y}}) \quad (22a)$$

$$= \mathbb{E}_{\tilde{\mathcal{D}}} \|Y_f \hat{g} - \mathbf{y}^r\|_Q^2 + \omega(U_f \hat{g}, Y_f \hat{g}) \quad (22b)$$

The optimization problem for training of neural network  $\tilde{F}_{\tilde{\theta}}$  without the steady-state reference inputs can be formulated as follows:

$$\min_{\tilde{\theta}} \tilde{\mathcal{L}} = \min_{\tilde{\theta}} \mathbb{E}_{\tilde{\mathcal{D}}} \|Y_f \hat{g} - \mathbf{y}^r\|_Q^2 + \omega(U_f \hat{g}, Y_f \hat{g}) \quad (23)$$

where  $\hat{g} = \tilde{F}_{\tilde{\theta}}(\mathbf{u}_{ini}, \mathbf{y}_{ini}, e_y | \tilde{\theta})$ .

The trained neural network  $\tilde{F}_{\tilde{\theta}}$  is used to output DeePC operator  $\hat{g}_k$ , at each sampling time instant  $k$ ,  $k \in \mathbb{Z}_{\geq 0}$ . The DeePC operator is used to generate the optimal control sequence  $\hat{\mathbf{u}}_k^*$  following:

$$\hat{\mathbf{u}}_k^* = U_f \hat{g}_k = U_f \tilde{F}_{\tilde{\theta}}(\mathbf{u}_{ini,k}, \mathbf{y}_{ini,k}, e_{y,k} | \tilde{\theta}^*) \quad (24)$$

where  $\tilde{\theta}^*$  is the well-trained parameters of neural network  $\tilde{F}_{\tilde{\theta}}$ . The first control action  $\hat{u}_{k|k}^*$  in  $\hat{\mathbf{u}}_k^*$  will be applied to drive the system to the desired operation condition.

## 7 Case study on gene regulatory network

### 7.1 Process description

A gene regulatory network (GRN) is a nanoscale dynamic system within synthetic biology [49, 50]. We consider a three-gene regulatory network, where both mRNA and protein dynamics display oscillatory behaviors. The transcription and translation dynamics within this GRN can be described by a discrete-time nonlinear system, given as follows [49, 50]:

$$x_{k+1}(i) = x_k(i) + \left( -\gamma_i x_k(i) + \frac{a_i}{K_i + x_k^2(j)} + u_k(i) \right) \cdot \Delta + \xi_k(i), \quad (i, j) = \{(1, 6); (2, 4); (3, 5)\} \quad (25a)$$

$$x_{k+1}(i) = x_k(i) + (-c_j x_k(i) + \beta_j x_k(j)) \cdot \Delta + \xi_k(i), \quad (i, j) = \{(4, 1); (5, 2); (6, 3)\} \quad (25b)$$

where  $x(i), i = 1, 2, 3$ , denote the concentrations of the mRNA transcripts for the three different genes;  $x(i), i = 4, 5, 6$ , denote the concentrations of the corresponding proteins for three genes;  $\xi(i), i = 1, \dots, 6$ , denote the independent and identically distributed (i.i.d.) uniform noise, that is,  $\xi(i) \sim \mathcal{U}(-\delta, \delta)$ ;  $u(i), i = 1, 2, 3$ , denote the number of protein copies per cell produced from a given promoter type during continuous growth;  $a_i, i = 1, 2, 3$ , denote the maximum promoter strength for their corresponding gene;  $\gamma_i, i = 1, 2, 3$ , denote the mRNA degradation rates;  $c_i, i = 1, 2, 3$ , denote the protein degradation rates;  $\beta_i, i = 1, 2, 3$ , denote the protein production rates;  $K_i, i = 1, 2, 3$ , denote the dissociation constants;  $\Delta$  denotes the discretization time step, which is also the sampling period.

The state variables of the system include the concentrations of the mRNA ( $x(i), i = 1, 2, 3$ ) and the concentrations of the proteins ( $x(i), i = 4, 5, 6$ ). The measured output variables are the protein concentrations  $x(i), i = 4, 5, 6$ , which are measured online using fluorescent markers. The control inputs  $u(i), i = 1, 2, 3$ , are light control signals that can induce the expression of genes through the activation of their photo-sensitive promoters.

### 7.2 Settings

#### 7.2.1 Control methods being evaluated

In this section, three controllers are developed based on the following three control approaches: the proposed Deep DeePC method, which is referred to as Deep DeePC as described by (17); the proposed Deep DeePC method with the proposed constraint handling scheme, which is referred to as constrained Deep DeePC as described by (20); and conventional DeePC, which is referred to as

Table 1: The initial state  $x_0$  and the four set-points  $x_{si}, i = 1, \dots, 4$ , of GRN.

	$x(1)$	$x(2)$	$x(3)$	$x(4)$	$x(5)$	$x(6)$
$x_0$	29.36	24.60	20.30	78.29	65.61	54.12
$x_{s1}$	22.47	17.29	11.65	59.93	46.10	31.06
$x_{s2}$	15.85	14.44	15.60	42.27	38.51	41.59
$x_{s3}$	16.67	70.86	13.26	44.45	18.90	35.35
$x_{s4}$	62.49	82.61	18.09	16.66	22.03	48.24

Table 2: Steady-state control inputs  $u_{si}, i = 1, \dots, 4$ , of GRN.

	$u(1)$	$u(2)$	$u(3)$
$u_{s1}$	0.7189	0.5536	0.3725
$u_{s2}$	0.5070	0.4620	0.4989
$u_{s3}$	0.5332	0.2266	0.4233
$u_{s4}$	0.1998	0.2632	0.5783

DeePC as described in (6).

### 7.2.2 Parameters

The following parameters are chosen for the three controllers to ensure a fair comparison:  $T = 200$ ,  $T_{ini} = 10$ ,  $N_p = 10$ ,  $Q = 5 \times I_{30}$ , and  $R = 1 \times I_{30}$ . Deep DeePC and constrained Deep DeePC use the same weighting matrices to penalize the violation of input and output constraints; specifically,  $P_u = 10 \times I_{30}$  and  $P_y = 10 \times I_{30}$ , respectively. The Hankel matrices  $U_p, U_f, Y_p$ , and  $Y_f$  are identical across all designs.

The neural network architecture accounting for the DeePC operator consists of an input layer, two hidden layers, and an output layer. The number of neurons in different layers of the neural network involved in Deep DeePC is 66-150-150-181. The network uses the rectified linear unit (ReLU) as the activation function after the input and hidden layers. The training process involves 1000 epochs with a batch size of 200. The Adam optimizer, with a learning rate of  $10^{-4}$ , is employed for training. To ensure a fair comparison, the constrained Deep DeePC model utilizes the same well-trained neural network as the Deep DeePC.

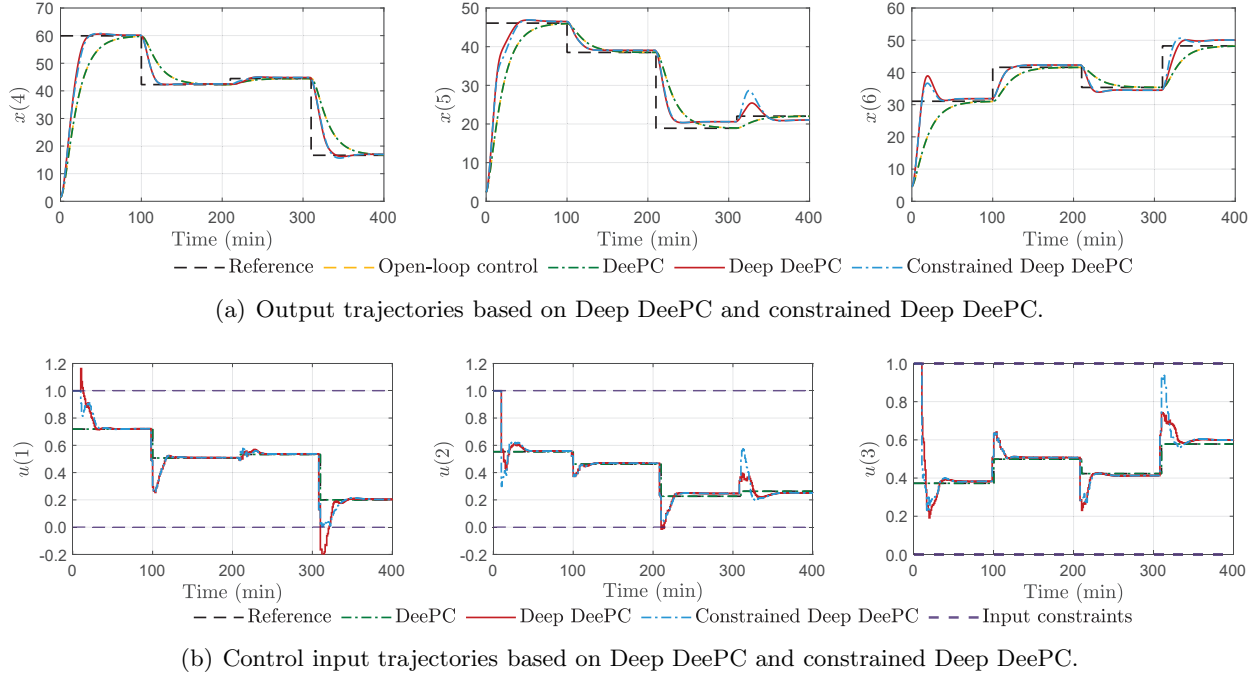


Figure 4: Output and control input trajectories of GRN under designs with reference input.

### 7.2.3 Simulation setting

In this study, the following system parameters are adopted for the GRN process:  $K_i = 1$ ,  $a_i = 1.6$ ,  $\gamma_i = 0.16$ ,  $\beta_i = 0.16$ ,  $c_i = 0.06$  ( $i = 1, 2, 3$ ),  $\delta = 0$ , and  $\Delta = 1$  min, which are the same as those in [50]. First, open-loop simulations are conducted using the first-principles model (25) to generate data. The generated data are used for two purposes: 1) to construct the Hankel matrices  $U_p, U_f, Y_p$ , and  $Y_f$ , and 2) to train the DeePC operator within the proposed framework.  $T = 200$  is used as we construct the Hankel matrices. The data size for training the neural network is  $10^4$ . The control inputs  $u(i)$ ,  $i = 1, 2, 3$ , are generated randomly following a uniform distribution with a prescribed range. Particularly,  $u(i) \in [0, 1]$ ,  $i = 1, 2, 3$ , and each of the inputs varies every 30 sampling periods.

During the online implementation, four open-loop stable steady states are considered as the set-points (i.e., the reference outputs) for the proposed controller to track. The tracking set-points are varied after every 100 sampling periods. The initial state  $x_0$  and the four set-points  $x_{s_i}$ ,  $i = 1, \dots, 4$ , are listed in Table 1. The control inputs  $u_{s_i}$ ,  $i = 1, \dots, 4$ , corresponding to the four set-points are listed in Table 2.

Table 3: Control performance comparison of GRN in terms of RMSEs.

	Open-loop	DeePC	Deep DeePC	Constrained Deep DeePC
RMSE	0.17217	0.17218	0.14062	0.14182

### 7.3 Control performance

Figure 4 shows the closed-loop output trajectories and control input trajectories obtained using Deep DeePC, constrained Deep DeePC, and conventional DeePC. Figure 4(a) illustrates the closed-loop output trajectories for the three controllers, alongside the open-loop output trajectories with steady-state reference inputs. Figure 4(b) displays the control input trajectories generated by the different controllers. All three DeePC designs can drive the system to the desired set-points. The proposed Deep DeePC (shown in red lines) and constrained Deep DeePC (shown in blue dashed lines) achieve faster convergence compared to conventional DeePC. In addition, as shown in Figure 4(b), the proposed Deep DeePC occasionally violates the input constraints, while the proposed constraint handling scheme ensures that the system constraints are satisfied throughout the entire online implementation.

To quantitatively assess the control performance, we calculate the root mean squared error (RMSE) for each controller. The RMSE is defined as  $\text{RMSE} = \sqrt{\frac{1}{n_y N_K} \sum_{k=1}^{N_K} \|y_k^r - y_k\|_2^2}$ , where  $N_K$  is the total number of sampling instants throughout the system operation. The RMSEs are computed using scaled system outputs. Table 3 presents the RMSE results for the three controllers, which demonstrate that both the proposed Deep DeePC method and the constrained Deep DeePC method outperform the conventional DeePC.

## 8 Case study on chemical process

In this section, we apply the proposed approach to a reactor-separator process. We examine two scenarios: when steady-state reference inputs are available and when they are unavailable.

### 8.1 Description of the process

This reactor-separator process consists of two continuous stirred reactors (CSTRs) and one flash tank separator. A schematic diagram of this process is presented in Figure 5. This process involves two irreversible reactions: reactant **A** converts into the desired product **B**, and **B** converts into the

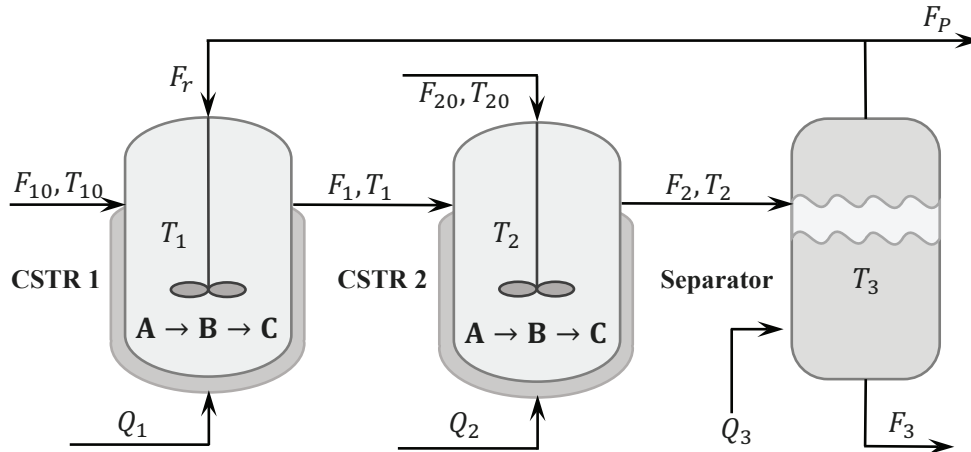


Figure 5: A schematic diagram of the reactor-separator process.

undesired side product **C** simultaneously.

In this process, the three vessels are interconnected through mass and energy flows. In the first reactor (CSTR 1), the input is pure reactant **A** at temperature  $T_{10}$  and volumetric flow rate  $F_{10}$ . In the second reactor (CSTR 2), the input includes the output stream from CSTR 1 and another stream containing pure **A** at temperature  $T_{20}$  and flow rate  $F_{20}$ . The effluent of CSTR 2 is sent to the separator with temperature  $T_2$  and flow rate  $F_2$ . The state variables of the reactor separator process include the mass fractions of reactant **A** ( $x_{A_i}, i = 1, 2, 3$ ), the mass fractions of the desired product **B** ( $x_{B_i}, i = 1, 2, 3$ ), and the temperature ( $T_i, i = 1, 2, 3$ ) in three vessels. The control inputs are the heat input rate  $Q_i, i = 1, 2, 3$ , to the three vessels. Typically, only the temperature  $T_i, i = 1, 2, 3$ , in three vessels are measured online using sensors. A detailed process description and the first-principles model of this process, which is used as the process simulator, can be found in [21,51]. The objective is to implement the proposed Deep DeePC approach to drive the process operation towards desired set-points by adjusting the heat input  $Q_i, i = 1, 2, 3$ , to the three vessels.

## 8.2 Problem formulation and simulation settings

### 8.2.1 Evaluated control methods

We consider five control methods to illustrate the effectiveness and superiority of the proposed methods: the proposed Deep DeePC method that uses steady-state reference inputs for offline training and online control implementation, which is referred to as Deep DeePC-I as described by (17); the proposed Deep DeePC method that does not require steady-state reference inputs for its

Table 4: The upper bounds and lower bounds of control inputs and controlled outputs of reactor-separator process.

	$Q_1$ (kJ/h)	$Q_2$ (kJ/h)	$Q_3$ (kJ/h)	$T_1$ (K)	$T_2$ (K)	$T_3$ (K)
Upper bounds	$3.1 \times 10^6$	$1.3 \times 10^6$	$3.1 \times 10^6$	494.0	486.0	488.0
Lower bounds	$2.6 \times 10^6$	$7.0 \times 10^5$	$2.6 \times 10^6$	480.0	472.0	474.0

online implementation, which is referred to as Deep DeePC-II as described by (24); Deep DeePC-I with the proposed constraint handling scheme, which is referred to as constrained Deep DeePC-I as described by (20); Deep DeePC-II with the proposed constraint handling scheme, which is referred to as constrained Deep DeePC-II; and conventional DeePC, which is referred to as DeePC as described in (6).

### 8.2.2 Parameter settings

The following parameters are chosen for all the five control methods to ensure a fair comparison:  $T = 200$ ,  $T_{ini} = 10$ ,  $N_p = 10$ ,  $Q = 5 \times I_{30}$ , and  $R = I_{30}$ . The four proposed Deep DeePC designs employ the same weighting matrices to penalize the violation of input and output constraints, which are  $P_u = 10 \times I_{30}$  and  $P_y = 10 \times I_{30}$ , respectively. The Hankel matrices  $U_p, U_f, Y_p$ , and  $Y_f$  remain the same for all the DeePC-based controllers.

The neural networks of Deep DeePC-I and Deep DeePC-II share a similar structure. Each neural network contains four layers: an input layer, two hidden layers, and an output layer. Both neural networks utilize the ReLU function as the activation function following the input and hidden layers. The training epoch is set to 1000, and the batch size is 200. The optimizer for the neural network training is Adam, and the learning rate is set as  $10^{-4}$ . The numbers of neurons in different layers of the neural networks involved in Deep DeePC-I and Deep DeePC-II are 66-150-150-181 and 63-150-150-181, respectively. For fair comparisons, constrained Deep DeePC-I uses the same well-trained neural network used in Deep DeePC-I (similarly to constrained Deep DeePC-II).

### 8.2.3 Data generation and process setting

First, open-loop process simulations are conducted using the first-principles model of the reactor-separator process to generate data. The generated batch open-loop data are divided into two parts for different tasks: one part is used to establish Hankel matrices  $U_p, U_f, Y_p$ , and  $Y_f$  for the DeePC design; the rest of the data are used for training the proposed controllers. The data size used for

Table 5: The initial state  $x_0$  and the five set-points  $x_{si}, i = 1, \dots, 5$ , of reactor-separator process.

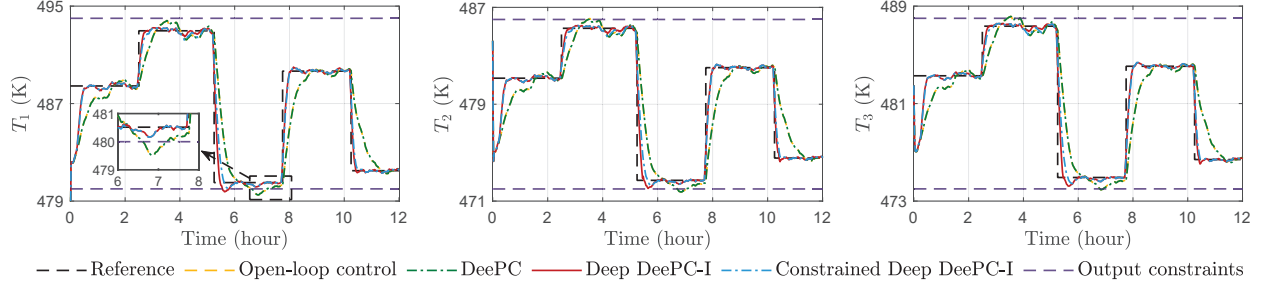
	$x_{A1}$	$x_{B1}$	$T_1$ (K)	$x_{A2}$	$x_{B2}$	$T_2$ (K)	$x_{A3}$	$x_{B3}$	$T_3$ (K)
$x_0$	0.1405	0.6370	475.2	0.1683	0.6240	484.2	0.0545	0.5886	482.5
$x_{s1}$	0.1436	0.6568	488.4	0.1644	0.6375	481.1	0.0510	0.6167	483.3
$x_{s2}$	0.1287	0.6420	493.0	0.1500	0.6230	485.3	0.0450	0.5843	487.4
$x_{s3}$	0.1757	0.6730	480.5	0.1961	0.6533	472.7	0.0650	0.6695	474.9
$x_{s4}$	0.1397	0.6534	489.7	0.1608	0.6341	482.0	0.0495	0.6086	484.1
$x_{s5}$	0.1705	0.6715	481.5	0.1904	0.6522	474.6	0.0624	0.6623	476.4

Table 6: Steady-state control inputs  $u_{si}, i = 1, \dots, 5$ , of reactor-separator process.

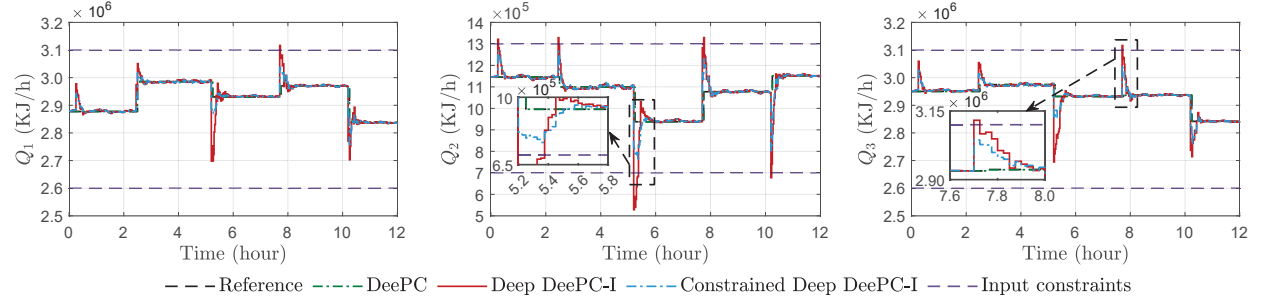
	$Q_1$ (kJ/h)	$Q_2$ (kJ/h)	$Q_3$ (kJ/h)
$u_{s1}$	$2.87743 \times 10^6$	$1.14562 \times 10^6$	$2.95015 \times 10^6$
$u_{s2}$	$2.98560 \times 10^6$	$1.09962 \times 10^6$	$2.97473 \times 10^6$
$u_{s3}$	$2.93024 \times 10^6$	$9.37622 \times 10^5$	$2.93181 \times 10^6$
$u_{s4}$	$2.97024 \times 10^6$	$1.07729 \times 10^6$	$2.93679 \times 10^6$
$u_{s5}$	$2.83789 \times 10^6$	$1.15186 \times 10^6$	$2.84174 \times 10^6$

constructing Hankel matrices is determined by the parameter  $T = 200$ , and the size of the training data is  $10^4$ . The sampling period is 0.025 hours. The heat inputs  $Q_i, i = 1, 2, 3$ , are generated randomly in a uniform distribution with the prescribed ranges and are varied every 2 hours. The upper bounds and lower bounds of the heat inputs and temperature outputs are shown in Table 4. Disturbances with bounded ranges are introduced into the process. The disturbances added to the mass fraction ( $x_{A_i}$  and  $x_{B_i}, i = 1, 2, 3$ ) and temperature ( $T_i, i = 1, 2, 3$ ) follow Gaussian distribution with zero mean and standard deviation of 1 and 5, respectively. The bounds for the disturbances in mass fraction and temperature are set to  $[-0.5, 0.5]$  and  $[-5, 5]$ , respectively.

During the online implementation, five open-loop stable steady states are considered as the set-points (i.e., the reference outputs) to illustrate our proposed methods. The tracking set-points are varied after every 2.5 hours. The initial state  $x_0$  and the five set-points  $x_{si}, i = 1, \dots, 5$ , are presented in Table 5. The control inputs  $u_{si}, i = 1, \dots, 5$ , corresponding to the five set-points are presented in Table 6.



(a) Output trajectories based on Deep DeePC-I and constrained Deep DeePC-I.



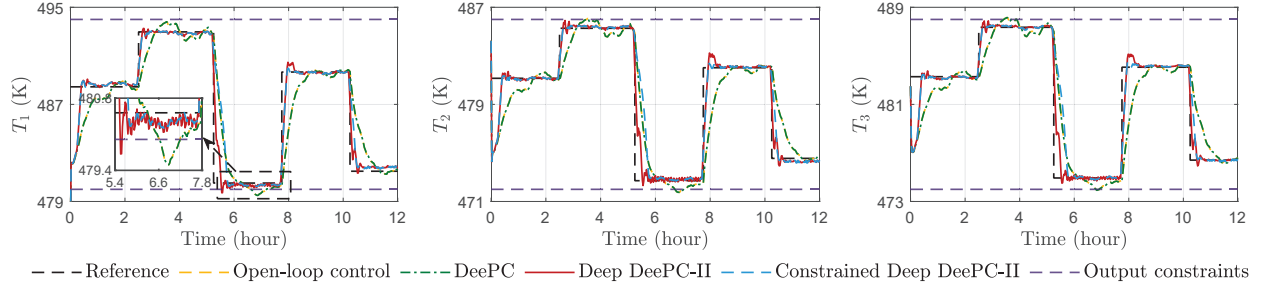
(b) Control input trajectories based on Deep DeePC-I and constrained Deep DeePC-I.

Figure 6: Output and control input trajectories of reactor-separator process under designs with reference input.

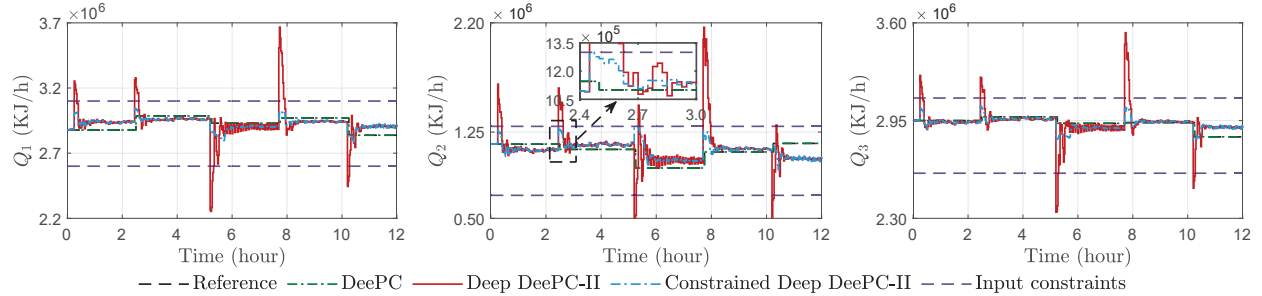
### 8.3 Results

First, we consider the case when the steady-state reference inputs corresponding to the set-points (reference outputs) are known. Two controllers are developed based on Deep DeePC-I and constrained Deep DeePC-I, respectively.

Figure 6 presents the closed-loop output trajectories and input trajectories obtained based on the Deep DeePC-I, constrained Deep DeePC-I, and conventional DeePC. Figure 6(a) presents the closed-loop trajectories of the output measurements based on the three controllers. In addition, the output trajectories based on open-loop control, with inputs being made the same as the steady-state reference inputs, are provided for comparison. Figure 6(b) presents the input trajectories by different controllers. All three DeePC designs can track the set-points and maintain the operation level close to the set-points. The proposed Deep DeePC-I and constrained Deep DeePC-I outperform the conventional DeePC by converging faster to the set-points. As shown in Figure 6(b), the control actions provided by Deep DeePC-I (shown in red lines) sometimes violate the input constraints. With the implementation of the proposed constraint handling scheme, constrained Deep DeePC-I (shown in blue dashed-dotted lines) ensures that the system constraints are satisfied throughout the entire operation.



(a) Output trajectories under the Deep DeePC-II and constrained Deep DeePC-II.



(b) Control input trajectories under the Deep DeePC-II and constrained Deep DeePC-II.

Figure 7: Output and control input trajectories of reactor-separator process under designs without reference input.

Next, we consider the case when the steady-state reference inputs  $\mathbf{u}^r$  are absent, and two controllers are developed based on Deep DeePC-II and constrained Deep DeePC-II, respectively. Figure 7 presents the closed-loop results obtained based on different controllers. Specifically, Figure 7(a) presents the output trajectories of Deep DeePC-II, constrained Deep DeePC-II, and conventional DeePC; Figure 7(b) presents the corresponding control input trajectories. All the controllers are able to steer the process states toward the desired set-points and maintain the process operation close to the set-points. The proposed Deep DeePC designs demonstrate superior control performance compared to the conventional DeePC design in terms of faster convergence speed. As shown in Figure 7(b), due to the absence of reference input, the control inputs provided by the Deep DeePC-II have a larger deviation from the steady-state reference inputs, as compared to the Deep DeePC-I design, which is designed and implemented with the steady-state reference inputs, as shown in Figure 6(b). Although the Deep DeePC-II exhibits larger deviations from the steady-state reference inputs and significant input constraint violations, the proposed constraint handling scheme in constrained Deep DeePC-II is able to provide control actions that consistently satisfy the corresponding hard constraints on system inputs and outputs.

To quantitatively assess and compare the control performance, we compute the RMSE for

Table 7: Control performance comparison in terms of RMSEs for the case with steady-state reference inputs.

	Open-loop	DeePC	Deep DeePC-I	Constrained Deep DeePC-I
RMSE	0.07537	0.07550	0.04194	0.04622

Table 8: Control performance comparison in terms of RMSEs for the case without steady-state reference inputs.

	Open-loop	DeePC	Deep DeePC-II	Constrained Deep DeePC-II
RMSE	0.07537	0.07550	0.04309	0.06079

each controller. The RMSEs are computed using scaled output values to mitigate the influence of multiple magnitudes of output variables that have different physical meanings. Table 7 presents the RMSE results for Deep DeePC-I and constrained Deep DeePC-I, where steady-state reference inputs are used for controller training and online implementation. Both Deep DeePC designs outperform the conventional DeePC. The constrained Deep DeePC-I shows a slightly higher RMSE compared to Deep DeePC-I, due to the enforcement of system constraints. Table 8 presents the RMSE results for Deep DeePC-II and constrained Deep DeePC-II, where steady-state reference inputs are absent. In this context, the proposed Deep DeePC-II and constrained Deep DeePC-II also provide improved performance compared to the conventional DeePC.

**Remark 1** *In real-world applications, it can be challenging or costly to measure certain state variables using hardware sensors in real-time. For example, measuring concentrations of substances often requires a lab analyzer, which can be time-consuming and presents challenges for implementing online control methods. It is worth noting that the proposed Deep DeePC method, owing to the adoption of the DeePC framework, requires only system output feedback (specifically, temperature measurements in the reactor-separator process). This approach offers enhanced practicality compared to optimal control methods that require full-state feedback.*

#### 8.4 Comparisons of computation time

We evaluate the computation time for conventional DeePC, Deep DeePC-I, and constrained Deep DeePC-I during online implementation. We evaluate the average computation time per step across 100 evaluation trials. Each evaluation trial starts with a different initial state and is subject to

Table 9: Comparison of computation time.

	DeePC	Deep DeePC-I	Constrained Deep DeePC-I
Time (s/step)	0.04877	0.00015	0.00334

Table 10: Computation times of conventional DeePC with varying  $T$  ( $T_{ini} = N_p = 10$ ).

$T$	200	400	600
Time (s/step)	0.04877	0.14146	0.30272

varying disturbances over a total of 500 sampling periods. The objective is to track the five set-points listed in Table 5. The experiments are conducted on a computer equipped with an Intel<sup>®</sup> Core<sup>™</sup> i9-13900 CPU with 24 cores and 128 GB of random access memory (RAM).

Table 9 presents the average computation time for different DeePC-based controllers. The proposed methods significantly reduce the average computation time compared to the conventional DeePC. Specifically, the average computation time for Deep DeePC-I, which does not involve online optimization, is reduced by 99.69% compared to the conventional DeePC. The average computation time for constrained Deep DeePC-I is reduced by 93.15% compared to the conventional DeePC. The constrained Deep DeePC-I requires more computation time than Deep DeePC-I since it involves the event-based constraint handling scheme. This scheme is activated to manage hard constraints at an average event rate of 19.84% across the 100 evaluation trials. The average computation time for a single execution of the constraint handling scheme in (19) is 0.01598 seconds, achieving a 67.23% reduction in computation time compared to a single execution of conventional DeePC in (12). This indicates that when the constraint handling scheme is activated, it solves a simpler optimization problem than the one associated with conventional DeePC.

We also assess how the parameters affect the computation time of conventional DeePC. Table 10 presents the average computation times for DeePC with different values of  $T$ . The results indicate that the computation time for the DeePC optimization problem increases rapidly as  $T$  increases. This suggests that the complexity of the conventional DeePC optimization problem in (12) is significantly influenced by the parameters  $T$ ,  $T_{ini}$ , and  $N_p$ . To satisfy the persistently exciting condition described in Definition 1,  $T$  generally needs to be made sufficiently large, which leads to increased computation time for DeePC. In contrast, the proposed Deep DeePC methods are minimally affected by these parameters ( $T$ ,  $T_{ini}$ , and  $N_p$ ), since either no optimization or only

low optimization needs to be solved during online implementation.

## 9 Conclusion

In this paper, we proposed a computation-efficient, deep learning-enabled DeePC control approach for nonlinear processes, referred to as Deep DeePC. Within the proposed framework, a deep neural network is used to output the DeePC operator  $g$  at each sampling instant, and the generated DeePC operator is then used to generate an optimal control input sequence. The parameters of this neural network can be trained using input and output data collected from open-loop process operations. During online implementation, the Deep DeePC framework leverages the trained neural network to directly output the DeePC operator. Therefore, online optimization required by conventional DeePC is bypassed. To further address constrained control problems, a constraint handling scheme was developed and integrated with the proposed Deep DeePC. The proposed approach was applied to both a gene regulatory network and a reactor-separator chemical process, good control performance was achieved in both case studies. The results demonstrated that this method can drive process operations toward desired set-points even when the reference inputs corresponding to those set-points are not provided. Additionally, the online computation time for executing the proposed Deep DeePC is significantly reduced compared to conventional DeePC. The constrained Deep DeePC can handle input and control constraints, while maintaining more efficient online computation as compared to conventional DeePC.

## Acknowledgment

This research is supported by the National Research Foundation, Singapore, and PUB, Singapore’s National Water Agency under its RIE2025 Urban Solutions and Sustainability (USS) (Water) Centre of Excellence (CoE) Programme, awarded to Nanyang Environment & Water Research Institute (NEWRI), Nanyang Technological University, Singapore (NTU). This research is supported by Ministry of Education, Singapore, under its Academic Research Fund Tier 1 (RS15/21 & RG63/22), and Nanyang Technological University, Singapore (Start-Up Grant). Any opinions, findings and conclusions or recommendations expressed in this material are those of the author(s) and do not reflect the views of the National Research Foundation, Singapore and PUB, Singapore’s National Water Agency.

## Data availability statement

The numerical data used to generate Figures 4, 6, 7, and Tables 3, 7, 8 are provided in the Supplementary Material. The compressed file contains data obtained from the case studies on the gene regulatory network and the reactor-separator process. This encompasses simulated historical open-loop data for neural network training, maximum and minimum values of states used for scaling, and the simulated closed-loop trajectories based on different control approaches (i.e., our proposed Deep DeePC, conventional DeePC, and open-loop control). The data can be used to reproduce and generate the figures and tables presented in this paper. Specifically, the RMSEs in Tables 3, 7, and 8 can be obtained using the reference trajectories and the trajectories provided by different controllers. Additionally, the Hankel matrices and the training data for the neural network can be constructed using historical open-loop data, following the instructions provided in this paper. The source code for our methods is available at <https://github.com/QiYuan-Zhang/Deep-DeePC>.

## Literature cited

- [1] Findeisen R, Allgöwer F. An introduction to nonlinear model predictive control. *21st Benelux Meeting on Systems and Control*. 2002;11:119–141.
- [2] Mayne DQ, Rawlings JB, Rao CV, Scokaert POM. Constrained model predictive control: Stability and optimality. *Automatica*. 2000;36(6):789–814.
- [3] Gräber M, Kirches C, Schlöder JP, Tegethoff W. Nonlinear model predictive control of a vapor compression cycle based on first principle models. *IFAC Proceedings Volumes*. 2012;45(2):258–263.
- [4] Palma-Flores O, Ricardez-Sandoval LA. Integration of design and NMPC-based control for chemical processes under uncertainty: An MPCC-based framework. *Computers & Chemical Engineering*. 2022;162:107815.
- [5] Findeisen R, Allgöwer F. Computational delay in nonlinear model predictive control. *IFAC Proceedings Volumes*. 2004;37(1):427–432.
- [6] Daoutidis P, Lee JH, Harjunkski I, Skogestad S, Baldea M, Georgakis C. Integrating operations and control: A perspective and roadmap for future research. *Computers & Chemical Engineering*. 2018;115:179–184.

- [7] Christofides PD, Scattolini R, De La Peña DM, Liu J. Distributed model predictive control: A tutorial review and future research directions. *Computers & Chemical Engineering*. 2013;51:21–41.
- [8] Daoutidis P, Zachar M, Jogwar SS. Sustainability and process control: A survey and perspective. *Journal of Process Control*. 2016;44:184–206.
- [9] Rajulapati L, Chinta S, Shyamala B, Rengaswamy R. Integration of machine learning and first principles models. *AIChE Journal*. 2022;68(6):e17715.
- [10] Markovsky I, Dörfler F. Behavioral systems theory in data-driven analysis, signal processing, and control. *Annual Reviews in Control*. 2021;52:42–64.
- [11] Lamnabhi-Lagarrigue F, Annaswamy A, Engell S, Isaksson A, Khargonekar P, Murray RM, Nijmeijer H, Samad T, Tilbury D, Van den Hof P. Systems & control for the future of humanity, research agenda: Current and future roles, impact and grand challenges. *Annual Reviews in Control*. 2017;43:1–64.
- [12] Tang W, Daoutidis P. Distributed adaptive dynamic programming for data-driven optimal control. *Systems & Control Letters*. 2018;120:36–43.
- [13] Tang W, Daoutidis P. Data-driven control: Overview and perspectives. *American Control Conference*. 2022;1048–1064, Atlanta, GA.
- [14] Hu C, Wu Z. Machine learning-based model predictive control of hybrid dynamical systems. *AIChE Journal*. 2023;69(12):e18210.
- [15] Wang X, Ayachi S, Corbett B, Mhaskar P. Integrating autoencoder with Koopman operator to design a linear data-driven model predictive controller. *The Canadian Journal of Chemical Engineering*. 2024.
- [16] Koopman BO. Hamiltonian systems and transformation in Hilbert space. *Proceedings of the National Academy of Sciences*. 1931;17(5):315–318.
- [17] Korda M, Mezić I. Linear predictors for nonlinear dynamical systems: Koopman operator meets model predictive control. *Automatica*. 2018;93:149–160.
- [18] Narasingam A, Kwon JSI. Koopman Lyapunov-based model predictive control of nonlinear chemical process systems. *AIChE Journal*. 2019;65(11):e16743.

- [19] Han Y, Hao W, Vaidya U. Deep learning of Koopman representation for control. *IEEE Conference on Decision and Control*. 2020;1890–1895, Jeju, Republic of Korea.
- [20] Han M, Li Z, Yin X, Yin X. Robust learning and control of time-delay nonlinear systems with deep recurrent Koopman operators. *IEEE Transactions on Industrial Informatics*. 2024;20(3):4675–4684.
- [21] Zhang X, Han M, Yin X. Reduced-order Koopman modeling and predictive control of nonlinear processes. *Computers & Chemical Engineering*. 2023;179:108440.
- [22] Abhinav N, Kwon JSI. Application of Koopman operator for model-based control of fracture propagation and proppant transport in hydraulic fracturing operation. *Journal of Process Control*. 2020;91:25–36.
- [23] Li X, Bo S, Zhang X, Qin Y, Yin X. Data-driven parallel Koopman subsystem modeling and distributed moving horizon state estimation for large-scale nonlinear processes. *AIChE Journal*. 2024;70(3):e18326.
- [24] Shi Y, Hu X, Zhang Z, Chen Q, Xie L, Su H. Data-driven identification and fast model predictive control of the ORC waste heat recovery system by using Koopman operator. *Control Engineering Practice*. 2023;141:105679.
- [25] Li Z, Han M, Vo DN, Yin X. Machine learning-based input-augmented Koopman modeling and predictive control of nonlinear processes. *Computers & Chemical Engineering*. 2024;191:108854.
- [26] Shi L, Karydis K. Enhancement for robustness of Koopman operator-based data-driven mobile robotic systems. *IEEE International Conference on Robotics and Automation*. 2021;2503–2510, Xi'an, China.
- [27] Cibulka V, Haniš T, Korda M, Hromčík M. Model predictive control of a vehicle using Koopman operator. *IFAC-PapersOnLine*. 2020;53(2):4228–4233.
- [28] Xiao Y, Zhang X, Xu X, Liu X, Liu J. Deep neural networks with Koopman operators for modeling and control of autonomous vehicles. *IEEE Transactions on Intelligent Vehicles*. 2022;8(1):135–146.

- [29] Marcos N, Lamine M. A robust data-driven Koopman Kalman filter for power systems dynamic state estimation. *IEEE Transactions on Power Systems*. 2018;33(6):7228–7237.
- [30] Zhao T, Yue M, Wang J. Deep-learning-based Koopman modeling for online control synthesis of nonlinear power system transient dynamics. *IEEE Transactions on Industrial Informatics*. 2023;19(10):10444–10453.
- [31] Xu Y, Wang Q, Mili L, Zheng Z, Gu W, Lu S, Wu Z. A data-driven Koopman approach for power system nonlinear dynamic observability analysis. *IEEE Transactions on Power Systems*. 2023;39(2):4090–4104.
- [32] Han M, Yao J, Law AWK, Yin X. Efficient economic model predictive control of water treatment process with learning-based Koopman operator. *Control Engineering Practice*. 2024;149:105975.
- [33] De Jong TG, Breschi V, Schoukens M, Lazar M. Koopman data-driven predictive control with robust stability and recursive feasibility guarantees. *arXiv preprint arXiv:2405.01292*. 2024.
- [34] Coulson J, Lygeros J, Dörfler F. Data-enabled predictive control: In the shallows of the DeePC. *European Control Conference*. 2019;307–312, Naples, Italy.
- [35] Huang L, Zhen J, Lygeros J, Dörfler F. Robust data-enabled predictive control: Tractable formulations and performance guarantees. *IEEE Transactions on Automatic Control*. 2023;68(5):3163–3170.
- [36] Zhang K, Chen K, Lin X, Zheng Y, Yin X, Hu X, Song Z, Li Z. Data-enabled predictive control for fast charging of lithium-ion batteries with constraint handling. *arXiv preprint arXiv:2209.12862*. 2022.
- [37] Willems JC, Rapisarda P, Markovsky I, De Moor BL. A note on persistency of excitation. *Systems & Control Letters*. 2005;54(4):325–329.
- [38] Garcia CE, Prett DM, Morari M. Model predictive control: Theory and practice—A survey. *Automatica*. 1989;25(3):335–248.
- [39] Zhang K, Zheng Y, Shang C, Li Z. Dimension reduction for efficient data-enabled predictive control. *IEEE Control Systems Letters*. 2023;7:3277–3282.

- [40] Carlet PG, Favato A, Torchio R, Toso F, Bolognani S, Dörfler F. Real-time feasibility of data-driven predictive control for synchronous motor drives. *IEEE Transactions on Power Electronics*. 2022;38(2):1672–1682.
- [41] Sader M, Wang Y, Huang D, Shang C, Huang B. Causality-informed data-driven predictive control. *arXiv preprint arXiv:2311.09545*. 2023.
- [42] Breschi V, Chiuso A, Formentin S. Data-driven predictive control in a stochastic setting: A unified framework. *Automatica*. 2023;152:110961.
- [43] Vahidi-Moghaddam A, Zhang K, Li Z, Wang Y. Data-enabled neighboring extremal optimal control: A computationally efficient DeePC. *IEEE Conference on Decision and Control*. 2023;4778–4783, Singapore.
- [44] Baros S, Chang CY, Colon-Reyes GE, Bernstein A. Online data-enabled predictive control. *Automatica*. 2022;138:109926.
- [45] Zhou Y, Lu Y, Li Z, Yan J, Mo Y. Learning-based efficient approximation of data-enabled predictive control. *arXiv preprint arXiv:2404.16727*. 2024.
- [46] Markovsky I, Rapisarda P. Data-driven simulation and control. *International Journal of Control*. 2008;81(12):1946–1959.
- [47] Proctor JL, Brunton SL, Kutz JN. Generalizing Koopman theory to allow for inputs and control. *SIAM Journal on Applied Dynamical Systems*. 2018;17(1):909–930.
- [48] Yin X, Qin Y, Liu J, Huang B. Data-driven moving horizon state estimation of nonlinear processes using Koopman operator. *Chemical Engineering Research and Design*. 2023;200:481-492.
- [49] Elowitz MB, Leibler S. A synthetic oscillatory network of transcriptional regulators. *Nature*. 2000;403(6767):335–338.
- [50] Han M, Euler-Rolle J, Katzschmann RK. DeSKO: Stability-assured robust control with a deep stochastic Koopman operator. *International Conference on Learning Representations*. 2022.
- [51] Liu J, De La Peña DM, Christofides PD. Distributed model predictive control of nonlinear process systems. *AIChE Journal*. 2009;55(5):1171–1184.